INVITED PAPER *Special Section on Microwave and Millimeter-Wave Technologies*

Class-E Power Amplifier with Improved PAE Bandwidth Using Double CRLH TL Stub for Harmonic Tuning

Shinichi TANAKA[†a)], ***Senior Member***, **Hirotaka ASAMI**[†*], ***and*** **Takahiro SUZUKI**[†**], ***Nonmembers***

SUMMARY This paper presents a class-E power amplifier (PA) with a novel harmonic tuning circuit (HTC) based on composite right-/left-handed transmission lines (CRLH TLs). One of the issues of conventional harmonically tuned PAs is the limited PAE bandwidth. It is shown by simulation that class-E amplifiers have potential of maintaining high PAE over a wider frequency range than for example class-F amplifiers. To make full use of class-E amplifiers with the superior characteristics, an HTC using double CRLH TL stub structure is proposed. The HTC is not only compact but also enhances the inherently wide operation frequency range of class-E amplifier. A 2-GHz 6 W GaN-HEMT class-E PA using the proposed HTC demonstrated a PAE bandwidth ($\geq$ 65%) of 380 MHz with maximum drain efficiency and PAE of 78.5% and 74.0%, respectively.

key words: *class-E, composite right-/left-handed transmission lines, power-added efficiency, power amplifier, harmonic tuning*

1. Introduction

As mobile communication systems are heading toward the next generation, RF front-end components are required to keep up with the increasing demands for higher frequency, wider bandwidth and lower distortion. Although such demands have adverse effect on the power efficiency of the power amplifiers (PAs), the efficiency is supposed to maintain its present status as the minimum requirement. In this sense, operating the existing PAs under harmonically-tuned conditions, such as in class-F [1], inverse class-F (class-F^{-1}) [2] or class-E [3] modes, is one of the promising solutions to this issue. To realize such amplifiers at operation frequency (f_0) in the low SHF-band (3–6 GHz), for example, it is necessary to control the harmonics ($2f_0$, $3f_0$) in the high SHF-band (6–30 GHz) with both high precision and minimum loss. For this reason, microstrip lines (MSLs), instead of lumped-elements, are commonly used for designing harmonic tuning circuits (HTCs) for such high frequencies. (The exceptions are PAs designed in MMIC technology, in which spiral inductors and MIM capacitors with good high frequency characteristics are available [4].)

There are, however, several issues involved in MSL-based HTCs. Firstly, in highly integrated PA architectures such as Doherty amplifiers [5] or envelope tracking amplifiers [6], there is little room for additional sub-circuits. Thus, the circuit size of the HTC needs to be significantly reduced, while at the same time maintaining the performance. Figures 1 (a) and 1 (b) is a typical configuration of conventional MSL-based HTC for class-F amplifier [7] and class-E amplifier [8], respectively. As for class-E amplifier, the harmonic load impedances jX_{L2} and jX_{L3} can have arbitrary values [9], depending on the switching capacitor (C_S). The HTCs of Figs. 1 (a) (top) and 1 (b) use stubs to generate $2f_0$ short and $3f_0$ short. Recently, we have reported class-F PAs using HTCs based on composite right-/left-handed transmission line (CRLH TL) stub technique [10], [11]. As shown in Fig. 1 (a) (bottom), it was demonstrated that two MSL stubs for generating $2f_0$ short and $3f_0$ short can be made into a single compact CRLH TL stub. However, the size of the HTC was not reduced in the direction along the input-output RF signal line, because the impedance transformer of quarter-wavelength ($\lambda/4$) was still needed to obtain the optimum harmonic load impedances for the FET.

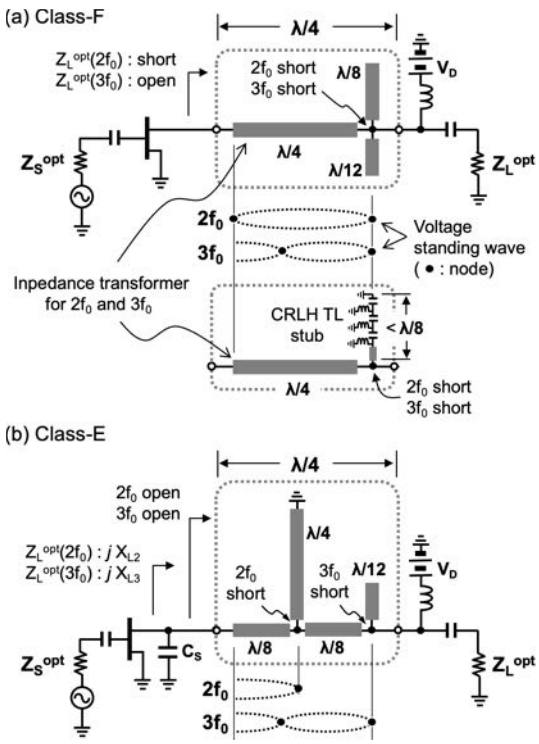

Fig. 1 Configuration of conventional harmonic tuning circuits for (a) class-F amplifier and (b) class-E amplifier.

Manuscript received January 21, 2022.
Manuscript revised February 26, 2022.
Manuscript publicized April 11, 2022.

[†]The authors are with the Department of Information and Communications Engineering, Shibaura Institute of Technology, Tokyo, 135–8548 Japan.
[*]Presently, with Sumitomo Electric Industries, Ltd.
[**]Presently, with Mitsubishi UFJ Trust Systems Co., Ltd.
a) E-mail: s-tanaka@shibaura-it.ac.jp

DOI: 10.1587/transele.2022MMI0002

The second issue is concerned with the operating bandwidth of PA. Since HTCs more or less use resonance to generate short or open for the harmonics, the bandwidth over which the harmonics are treated appropriately tends to be limited. Under such circumstances, operating the harmonically-tuned amplifiers in continuous mode has attracted much attention as techniques for maintaining the harmonically-tuned condition over an extremely wide frequency band [12], [13]. However, the continuous mode amplifiers generally require LPF type circuits occupying large circuit size for controlling both fundamental and harmonic frequencies. Thus, there is still demand for wideband PAs that can be realized without sacrificing the circuit size.

The purpose of this work is to present a class-E PA with improved PAE bandwidth, realized by a compact HTC using double CRLH TL stub. Part of the work was originally presented in [14], but no details were given as to why class-E mode was chosen for the amplifier design. In this work, we show that class-E mode has advantage over other common operation classes, such as class-F, in terms of PAE bandwidth. The paper is organized as follows. In Sect. 2, based on some simulation results, the issues involved in designing PA using HTC are discussed. In Sect. 3, after a brief review of the CRLH TL stub techniques, we present a new method of using CRLH TLs for class-E amplifiers. Finally, in Sect. 4 experimental results on the prototype class-E PA are demonstrated.

2. Design Issues of Harmonically Tuned PA

2.1 Circuit Size

In designing HTCs for cellular phone systems, distributed element circuits have the advantage over lumped element circuits, because the harmonic frequencies may reach frequencies as high as > 6 GHz. However, the wavelength of the fundamental frequency is not short enough to realize a compact circuit size if designed based fully on MSLs. Such conflicting demands for performance and circuit size becomes even more stringent for HTCs, which have to meet the load impedance conditions for at least two harmonics.

For example, in Figs. 1 (a) and 1 (b), the RF shorts at the harmonics (generated by the stubs) are transformed to the desired load impedances $Z_L^{opt}(2f_0)$ and $Z_L^{opt}(3f_0)$ using the impedance transformer. The harmonics control scheme well exploits the basic characteristics of the MSL, *i.e.* linear relationship between phase and frequency as well as the periodicity of the voltage standing wave. However, such conventional HTCs use longer MSLs than are naturally necessary for individually treating the impedances at $2f_0$ and $3f_0$. For instance, in Fig. 1, $\lambda/4$-length MSLs are used for transforming $3f_0$-short to $3f_0$-open even though it suffices to use $\lambda/12$-length MSL if only $3f_0$ is to be taken care of. Also, in Fig. 1 (b) a $\lambda/4$ short-ended stub is used to generate $2f_0$ short, while at the same time making the impedance looking into the stub open at $3f_0$ so as not to disturb the transformation of $3f_0$ impedance. Such redundant circuit designs increases the circuit size, and this comes out of necessity to deal with $2f_0$ and $3f_0$ simultaneously.

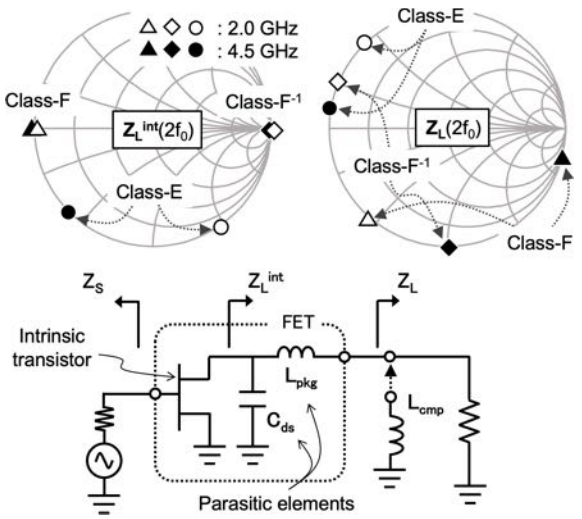

Fig. 2 Method of finding the harmonic load impedances for class-F, class-F^{-1} and class-E amplifier operation, when using FET with parasitic elements. Detailed parasitic network for FET used in this work was obtained from [17].

2.2 Power Efficiency Bandwidth

In general, the harmonic tuning technique improves the maximum PAE, but the efficiency bandwidth is limited unless a continuous class-F mode [12], for instance, is used. Another concern is that, from time to time, input harmonic tuning becomes necessary to make full use of the output harmonic tuning [15], [16]. Thus, when controlling the harmonics at both input and output side of the FET, the bandwidth of high-efficiency operation may be further restricted. Hence the question arises: on what conditions becomes the input harmonic tuning necessary?

To find a clue for the answer, we compared 2 GHz and 4.5 GHz amplifiers operating in class-F, class-F^{-1} and class-E modes. The simulation method is illustrated in Fig. 2. As for class-E amplifier, a shunt inductor L_{cmp} was used to compensate part of the drain-source capacitance of the FET (C_{ds}) for obtaining optimum switching capacitor C_S. In the simulation, no circuit components were used, except for the FET model of GaN HEMT (CGH40010F) and the shunt inductor L_{cmp}. Hence, the impedances, $Z_S(f_0)$, $Z_S(2f_0)$, $Z_L(f_0)$, $Z_L(2f_0)$ and $Z_L(3f_0)$, were treated numerically. To make the amplifiers operate accurately in class-F, class-F^{-1} and class-E modes, the harmonic load impedances $Z_L(2f_0)$ and $Z_L(3f_0)$ were tuned so that the impedances at the intrinsic FET plane, $Z_L^{int}(2f_0)$ and $Z_L^{int}(3f_0)$, satisfy the theoretical harmonic load conditions for each operation class. To this end, we used a parasitic network model for the FET of CGH40010F [17]. It can be seen from Fig. 2 that, at the high frequencies of $2f_0$ and $3f_0$, Z_L and Z_L^{int} differ significantly from each other. The final step of the simulation was to optimize $Z_S(f_0)$ and $Z_L(f_0)$, as well as $Z_S(2f_0)$ (op-

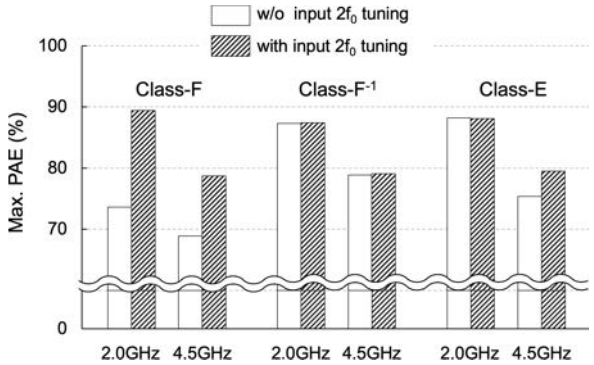

Fig. 3 Comparison of maximum PAE's for amplifiers with and without input second harmonic tuning. When input harmonic tuning was not used, $Z_S(2f_0)$ was set to 50 Ω.

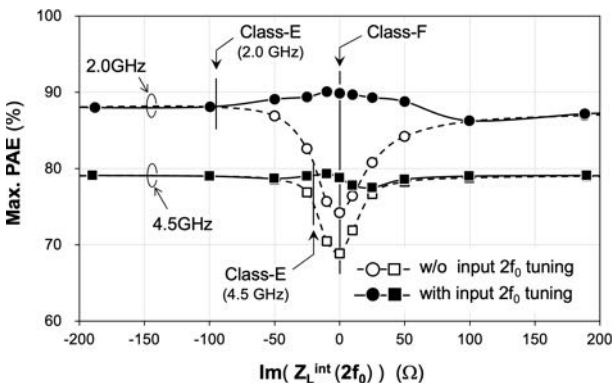

Fig. 4 Simulated maximum PAE for varying second harmonic load impedance at the intrinsic FET plane. Vertical bars denote the positions of optimum load impedances for class-E and class-F amplifiers.

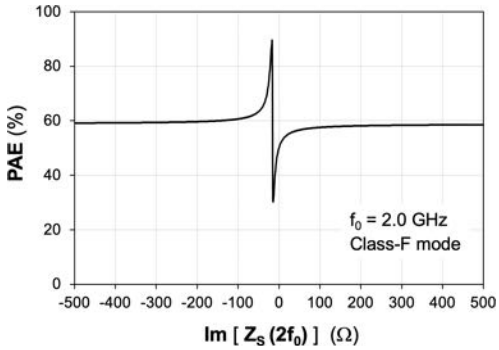

Fig. 5 Simulated PAE for varying second harmonic source impedance. The harmonic load impedances for the intrinsic FET are set for class-F operation.

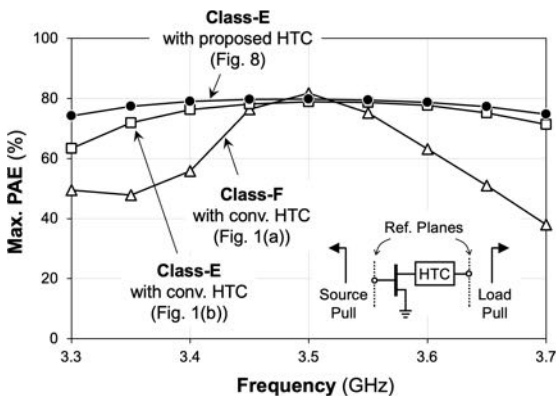

Fig. 6 Simulated maximum PAE versus frequency for class-F and class-E amplifiers.

tional) for maximum peak PAE. When tuning $Z_S(2f_0)$, only the imaginary part of $Z_S(2f_0)$ was optimized while the real part was fixed at zero. Otherwise, $Z_S(2f_0)$ was set to 50 Ω.

Figure 3 summarize the maximum power-added efficiency (PAE) values obtained for amplifiers with different operation classes. It can be seen that, in the case of class-F amplifier, PAE is significantly degraded unless $Z_S(2f_0)$ is appropriately tuned. In contrast, class-F^{-1} and class-E amplifiers do not rely on input harmonic tuning, except for the 4.5 GHz class-E amplifier, in which case the PAE is slightly improved by optimizing $Z_S(2f_0)$. Comparing Fig. 2 and Fig. 3, it can be speculated that $Z_S(2f_0)$ influences PAE if the following conditions are satisfied:

$$Im[Z_L^{int}(2f_0)] \; < \; 50\,\Omega. \tag{1}$$

To see if (1) applies to general cases, $Im[Z_L^{int}(2f_0)]$ was swept from $-j\,200\,\Omega$ to $j\,200\,\Omega$, as shown in Fig. 4. It can be seen that the above rule holds true not only for special harmonic load conditions of $Z_L^{int}(2f_0) = 0\,\Omega$ or $\infty\,\Omega$, as in class-F or class-F^{-1} amplifiers, but also for harmonic load conditions using arbitrary values of $Im[Z_L^{int}(2f_0)]$ [9], [16].

From Figs. 3 and 4, it can be seen that the PAE for 2-GHz class-F amplifier with input harmonic tuning is slightly higher than the PAE's for 2-GHz amplifiers operating in class-E or class-F^{-1} (whatever the input harmonic tuning). Thus, by tuning the 2nd harmonic source impedance $Z_S(2f_0)$ the peak PAE is surely enhanced, but the conditions for the high PAE become unstable. This is shown in Fig. 5, which plots the simulated PAE of 2-GHz class-F amplifier for varying $Z_S(2f_0)$ value. As can be seen, not only is the range of $Z_S(2f_0)$ for maximum PAE extremely narrow, but also a slight deviation of $Z_S(2f_0)$ from the peak PAE point can degrade the efficiency significantly. As a result, the PAE bandwidth becomes limited. Such phenomenon is also seen in amplifiers with reactive harmonic termination [16].

Figure 6 compares the frequency dependence of PAE for class-F and class-E amplifiers. For now, let us focus on amplifiers using conventional HTCs of Figs. 1 (a) and 1 (b). After the HTCs were designed for $f_0 = 3.5$ GHz, the optimum load impedance for f_0 and the source impedances for f_0 and $2f_0$ were obtained at the reference plane (see inset of Fig. 6). Then the frequency was swept from 3.3 GHz to 3.7 GHz, while the impedances were fixed. Comparing the plots for class-E and class-F amplifiers using conventional HTCs, it can be seen that for the class-E case high PAE (*e.g.* ≥ 70%) is maintained over wider bandwidth, even though the PAE's for the two amplifiers are similar at the center frequency. The wider bandwidth for class-E amplifier is partly due to the HTC design with less redundancy

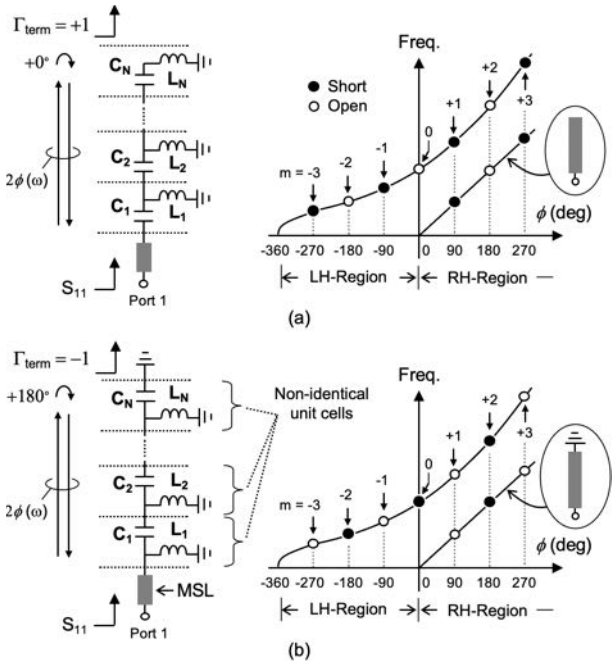

Fig. 7 One-port CRLH TLs of (a) C-first type and (b) L-first type. m denotes the order of the resonance mode. The dispersion diagrams for CRLH TLs are illustrated for $N = 2$. For comparison, dispersion diagrams for conventional MSLs with 50 Ω impedance are also shown.

and partly due to the fact that the amplifier does not rely on input harmonic tuning. From the findings obtained in this section, it can be concluded that class-E amplifier has great potential of operating with high efficiency over wide bandwidth.

3. Principle and Simulation of HTC

In this section, we show how CRLH TL stub can be used to design HTC for class-E amplifier without redundancy and thus with a compact circuit size.

3.1 Fundamentals of CRLH TL Stubs

CRLH TLs have attracted wide interests for microwave circuit application, because the phase-frequency relationship (dispersion diagram) can be engineered to design unique circuits that are difficult to realize using MSLs. However, if the CRLH TLs is used as two-port TLs, as usual, there are many design constraints. For example, to realize ideal signal transmission (low loss and low reflection), arranging symmetric unit cells in a periodic manner is a prerequisite for designing CRLH TL [18]. As a result, CRLH TLs are often forced to use identical unit cells, even though it is not a necessity for CRLH TLs. Thus, the potential offered by CRLH TLs have not necessarily been fully utilized.

The proposed HTC uses one-port CRLH TLs as stub lines [11], [19]. Figure 7 is a schematic illustration of one-port CRLH TLs. First of all, one-port CRLH TL is not a "transmission line" as it literally means. So, it is not the impedance, but only the phase that matters in designing the structure. Consequently, the unit cells of one-port CRLH TL do not have to be identical nor they have to be symmetric. The dispersion diagram $\phi(\omega)$ for one-port CRLH TL can be defined using S-parameters as:

$$S_{11}(\omega) = e^{-2j\phi(\omega)} \cdot \Gamma_{term}, \tag{2}$$

where Γ_{term} is the reflection coefficient at the terminal of one-port CRLH TL. As shown in Fig. 7, the dispersion curve extends continuously from the LH region to the right-handed (RH) region as the frequency is increased. It is not necessary to cope with the bandgap issue involved in two-port CRLH TLs. The resonance modes of the CRLH TL stub providing short and open occur alternately with 90° phase interval. (When we cite "short" or "open", we refer to the impedance at the port looking into the one-port CRLH TL.) In the dispersion diagram, the phase range of the LH region (Brillouin zone) depends on the unit cell number N. Thus, while the RH region comprises infinite number of positive-order resonance modes ($m > 0$), there are only $2N - 1$ number of negative-order resonance modes ($m < 0$).

What is unique about one-port CRLH TL is that the characteristics depends on which of the elements, L or C, comes first looking from the input port. As shown in Fig. 7, when a "C-first" CRLH TL stub is used, the fundamental resonance mode (with the lowest frequency) provides an impedance of short. On the other hand, the same resonance mode of an "L-first" CRLH TL gives rise to open at the port. Thus the CRLH TL of C-first type ($\Gamma_{term} = 1$) and L-first type ($\Gamma_{term} = -1$) corresponds to open-ended and short-ended MSL stub, respectively. The CRLH TL stub of L-first type can serve as a DC biasing circuit, because the inductor L_1 is DC-connected to the main RF signal line [11].

3.2 Operation Principle

Figure 8 represents the configurations of the proposed HTC, consisting of two CRLH-TL stubs and MSLs as impedance transformers. Unlike the conventional HTC (Fig. 1 (b)), in the proposed HTC the stub for $3f_0$ short (Stub-1) is placed in between the FET and the stub for $2f_0$ short (Stub-2). The $2f_0$ short due to Stub-2 is transformed to open at the FET by MSL of $\lambda/8$ without being disturbed by Stub-1. This becomes possible because Stub-1 is also designed to provide open at $2f_0$. Both $3f_0$ short (due to Stub-1) and $2f_0$ short (due to Stub-2) are transformed to open at the FET with minimum length of $\lambda/12$ and $\lambda/8$ ($= \lambda/12 + \lambda/24$), respectively. As a result, the size of the HTC along the input-output path becomes $\lambda/8$, which is half the size of the conventional HTC (Fig. 1 (b)).

As for Stub-2, we could have used $\lambda/8$-length open-ended MSL stub, but CRLH TL stub was chosen not only to shrink the stub length, but also to allow for supplying DC bias to the FET [11]. This eliminates the need to save area for dedicated DC biasing circuit, thus contributing to reduction of the whole amplifier circuit size. For connecting Stub-2 to DC supply, shunt capacitor C_{RF} is used to define

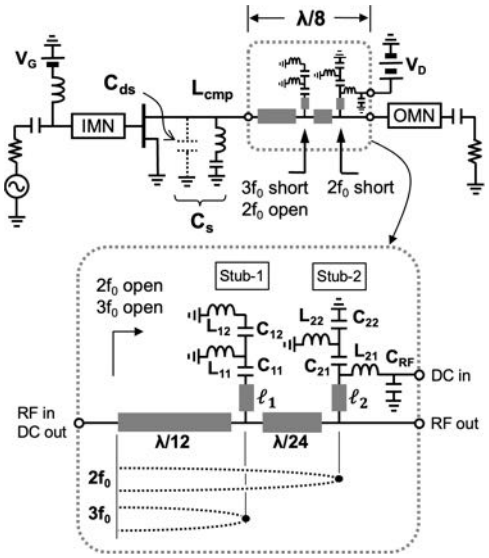

Fig. 8 Configuration of class-E amplifier using proposed HTC.

the inductance of L_{21} at the RF frequency band.

3.3 Design Method

The proposed HTC was designed for $f_0 = 2$ GHz. Figure 9 shows the simulated frequency response of the S_{11} phase for the one-port CRLH TLs. The phase was then transformed to dispersion diagram for Stub-1 and Stub-2 using (2). The dispersion diagrams thus obtained is shown in Fig. 10. Also shown in Fig. 10 are $|S_{21}|$ frequency responses for Stub-1 and Stub-2. As can be seen, at $2f_0$ (= 4 GHz), the open for Stub-1 overlaps the short for Stub-2, so the two stubs are independent of each other in terms of their effect on the 2nd harmonic load impedance of the FET.

As for Stub-1, the resonance mode of $m = -3$ (for short) is not in use. To make sure that the unwanted resonance does not affect the characteristics of the HTC within the operating band, the Q-factor for $m = -3$ resonance was intentionally increased by decreasing the dispersion gradient. On the contrary, to increase the bandwidth for harmonic tuning the gradient at the resonances of m = -1 (for Stub-1) and $m = -2$ (for Stub-2) were increased. The capability of customizing the bandwidth for each resonance mode is another advantage of CRLH TL stub using non-periodic structure.

3.4 Effect on Amplifier Performance

To verify the effect of the proposed HTC on the amplifier performance, a load pull simulation was performed for FET combined with the HTC as mentioned. As can be see from Fig. 6, the proposed HTC showed the same maximum PAE as that obtained for conventional HTC for class-E amplifier. As for the PAE bandwidth, there was some expectation that the bandwidth is improved by the proposed HTC, because the impedances for $2f_0$ and $3f_0$ are transformed with MSLs of minimum length. In fact, it can be seen that the

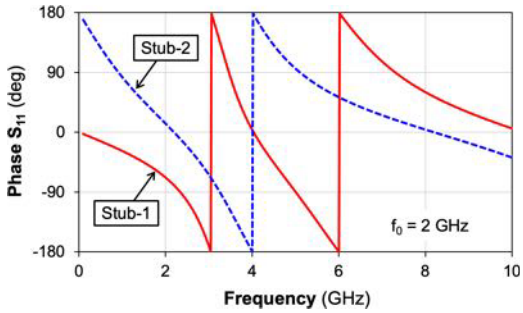

Fig. 9 Simulated frequency response of S_{11} phase for one-port CRLH TLs used in (a) Stub-1 and (b) Stub-2.

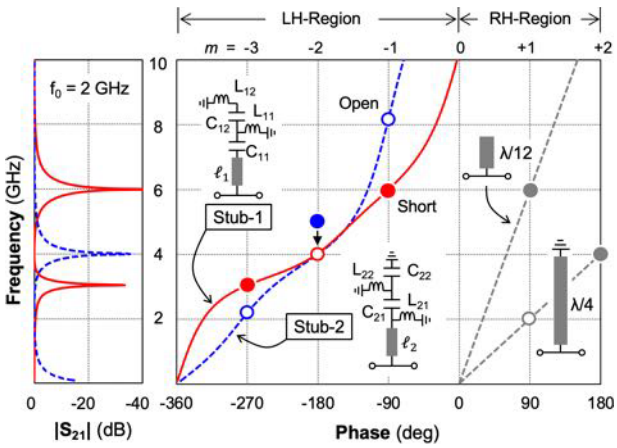

Fig. 10 Simulated $|S_{21}|$ frequency response for Stub-1 and Stub-2 and dispersion diagrams of corresponding one-port CRLH TLs. Solid circles and open circles denote short and open, respectively. The design parameters are: $C_{11} = 0.4$ pF, $C_{12} = 0.3$ pF, $C_{21} = 0.6$ pF, $C_{22} = 0.1$ pF, $L_{11} = 2.7$ nH, $L_{12} = 1.0$ nH, $L_{21} = 5.4$ nH, $L_{22} = 1.4$ nH, $\ell_1 = 21°$ and $\ell_2 = 18°$. For comparison, dispersion diagrams for MSL stubs in Fig. 1 (b) are also shown.

PAE bandwidth for the proposed HTC is slightly increased from that of the conventional HTC for class-E amplifier. The reason for the modest improvement is that the impedance transformer length for $2f_0$ was already minimum ($\lambda/8$) for the conventional HTC, so the effect of the circuit design improvement was only about $3f_0$. Even so, the proposed HTC performs just as well or better than the conventional HTC in spite of the small circuit size.

4. Experimental Results

4.1 Harmonic Tuning Circuit

Before testing the class-E PA, a stand-alone HTC for 2-GHz applications was fabricated and measured. Figure 11 shows the picture of the circuit fabricated on Panasonic R-5775 substrate ($h = 0.63$ mm, $\epsilon_r = 3.6$, $tan\,\delta = 0.002$). The CRLH TL stubs were initially designed using ADS circuit simulator. Next, the circuit layout was optimized using EM/circuit co-simulation. The non-ideal characteristics of the 1005-size multi-layer ceramic capacitors (MLCCs) was taken into account by using the equivalent circuit models provided by

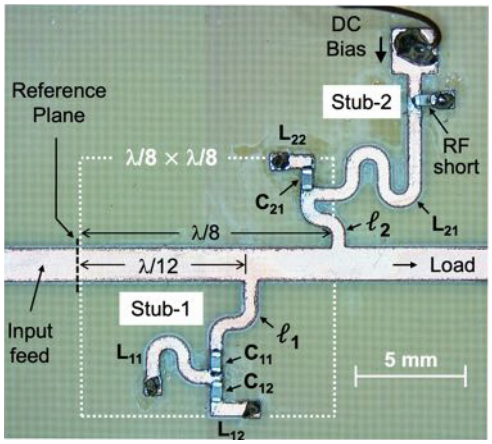

Fig. 11 Picture of fabricated harmonic tuning circuit. Shunt inductor L_{cmp} is not included in the present prototype circuit.

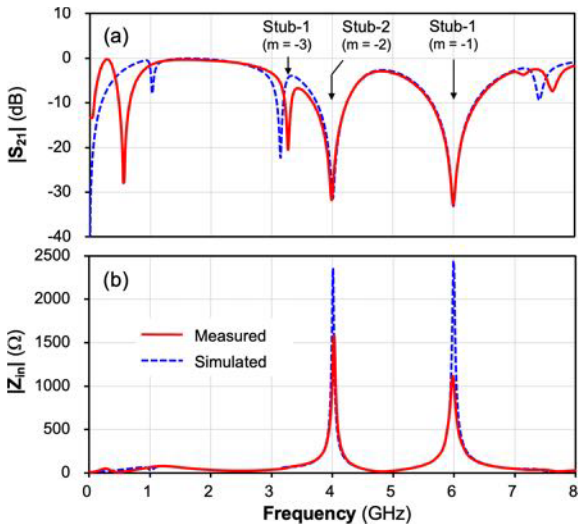

Fig. 12 Measurement results of $|S_{21}|$ and $|Z_{in}|$ for fabricated HTC.

the manufacturer. As for the capacitance of C_{22} in Fig. 8, instead of using MLCC, the fringing capacitance was used. The fringing effect of the MSL is naturally taken into account in the EM simulation. The shunt capacitor C_{RF} of 1.2 pF becomes an ideal short at around 4 GHz ($2f_0$) due to self-resonance of the MLCC. The shunt inductors comprising the CRLH TL stubs were realized using short-ended MSLs with characteristics impedance of 85 Ω. Considering that the inductor L_{21} can be laid out on the left-hand side of Stub-2, the HTC effectively fits in the area of $\lambda/8 \times \lambda/8$.

Figure 12 (a) shows the S-parameter measurement results for the fabricated HTC. To obtain the S-parameters at the reference plane, the input feed was de-embedded from the measured S-parameters. The transmission zeros at 4 GHz and 6 GHz results from the resonance modes of Stub-2 ($m = -2$) and Stub-1 ($m = -1$), respectively. Regarding the transmission zero at around 3.2–3.3 GHz due to Stub-1 ($m = -3$), there is a discrepancy between measurement and simulation. This is presumably because the resonant frequency has become sensitive to parameter variations, as a result of the intentionally increased Q-factor. In any case, this particular resonance mode is not used in the present design, so the slight frequency shift does not become a problem. There are other spurious responses at around 0.6 GHz and 7.5 GHz. The former is related to resonance in the DC bias feed line including L_{21} and ℓ_1. The latter is due to self-resonance of the capacitor C_{21}. With the exception of the spurious responses which are under control, the measurement is in good agreement with the simulation, particularly at around 2 GHz, 4 GHz and 6 GHz.

As can be seen from Fig. 11, the RF signal path for f_0 in the present HTC is a short and simple straight line. Thus, the insertion loss at f_0 is expected to be reasonably low. In fact, the measured insertion loss, calculated as:

$$I.L. = \frac{|S_{21}|^2}{1 - |S_{11}|^2}, \tag{3}$$

was estimated to be less than 0.1 dB. Figure 12 (b) shows the input impedance of the HTC:

$$|Z_{in}| = Z_0 \left| \frac{1 + S_{11}}{1 - S_{11}} \right|, \tag{4}$$

where Z_0 is the characteristic impedance of the impedance transformer (50 Ω for the present HTC). It can be seen that, at $2f_0$ and $3f_0$, $|Z_{in}|$ exceeds 1000 Ω, indicating that the harmonics conditions for class-E amplifier operation are well satisfied.

4.2 Power Amplifier

The proposed HTC was applied to a 2-GHz Class-E PA. The amplifier was simulated using non-linear model of GaN HEMT device (CGH40006P) from Cree Inc. Load pull analysis was performed for the FET combined with switching capacitor (C_S) as well as the HTC. The optimum value for C_S was obtained by tuning the shunt inductor L_{cmp} for partially compensating the capacitance of C_{ds} (Fig. 1).

Figure 13 shows the simulated PAE of the amplifier as a function of L_{cmp}. As can be seen, PAE increases with increasing L_{cmp} until it reaches maximum when L_{cmp} becomes 2.6 nH. As L_{cmp} is further increased, PAE decreased gradually. Figure 14 shows the output power (P_{out}) and PAE load-pull contours for L_{cmp} of 2.6 nH, 3.0 nH, 3.4 nH and 4.6 nH. It can be seen that with increasing L_{cmp} the optimum load points for Pout and PAE become closer to each other. Furthermore, it can be seen that L_{cmp} must be equal to or greater than 3.0 nH if the output matching network for maximum PAE is to be made compact. Considering the trade-off relation between PAE, Pout and the circuit size, L_{cmp} of 3.4 nH was chosen for the amplifier design.

Figure 15 shows the photograph of the fabricated PA. The input matching network was designed based on conventional MSL technique. As mentioned in Sect. 2, no input harmonic tuning was used for the present class-E PA. As for the output matching network, it can be seen that the

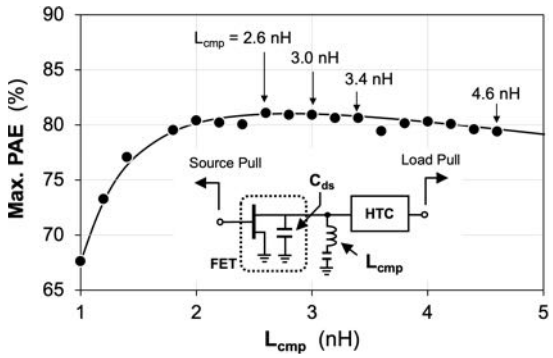

Fig. 13 Simulated maximum PAE of class-E PA as a function of shunt-inductance L_{cmp}. FET bias conditions are $V_G = -3.1$ V and $V_D = 28$ V.

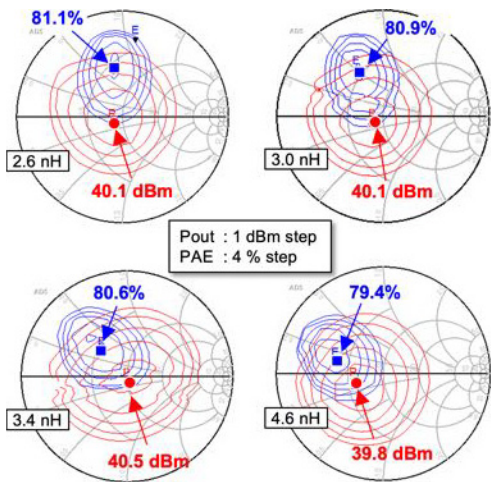

Fig. 14 Output power and PAE load-pull contours.

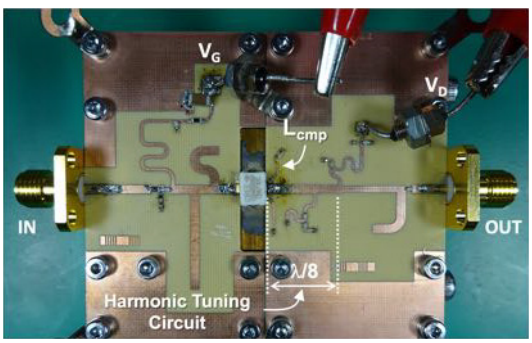

Fig. 15 Picture of fabricated 2-GHz-band class-E power amplifier.

drain bias is supplied to the FET via the CRLH TL stub (Stub-2), thus saving the area for dedicated biasing circuit. Figure 16 plots the measured power performance of the amplifier. The PAE obtained for 2 GHz was 74.0% when the drain efficiency and P_{out} were 78.5% and 38.6 dBm, respectively.

Figure 17 shows the frequency dependence of maximum PAE for fixed input power of 25 dBm. For comparison, the results from our previous work on class-F PA [11] are also shown. It can be seen that the bandwidth for

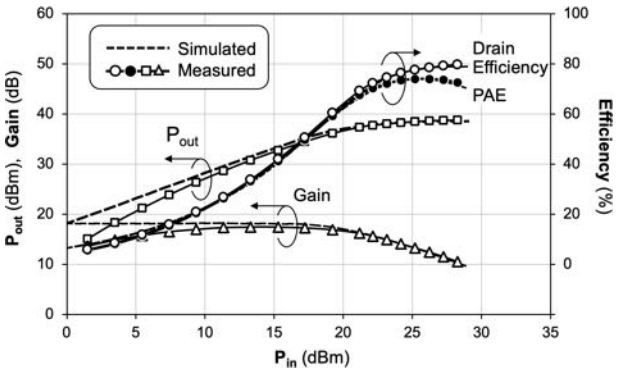

Fig. 16 Power performance of fabricated PA measured at 2 GHz. FET bias conditions are $V_G = -3.1$ V and $V_D = 28.0$ V.

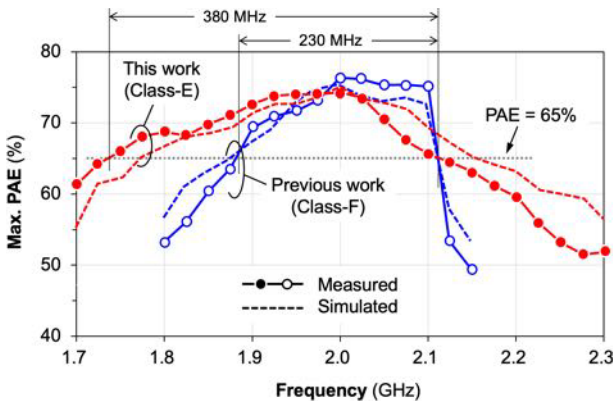

Fig. 17 Frequency dependence of maximum PAE of fabricated class-E PA. For comparison, the result of our previous work [11] is also shown. FET bias conditions are $V_G = -3.1$ V and $V_D = 28$ V. Input power was fixed at 25 dBm.

PAE ≥ 65% is around 1.6 times higher for the present class-E PA. The PA of class-F uses input harmonic tuning, so the peak PAE is higher compared to that of the class-E PA. However, as the frequency is increased from the center frequency (2 GHz), the efficiency for the class-F PA drops significantly at 2.1 GHz, where the second harmonic impedance shifts from the optimum to the worst conditions, as shown in Fig. 5.

5. Conclusion

We have shown that class-E amplifiers have great potential of maintaining high PAE over wide frequency range, because they do not rely on input harmonic tuning. Another reason is that the HTC for class-E amplifier can potentially be designed with minimal redundancy in terms of the impedance transformer length. To take advantage of such superior characteristics of class-E amplifiers, the objective of the present work was to realize a compact HTC for class-E PA. The task, however, is difficult to accomplish using MSL-based design because of the constraints rooted in the property of right-handed electromagnetic wave. Accordingly, we proposed an HTC using double CRLH TL

stub, which eliminates the redundancy used in conventional HTCs to control the 2nd and 3rd harmonics. The key to realizing such multiple frequency control scheme was to use the unique features of one-port CRLH TLs with non-periodic structure. While the demands imposed by advanced wireless technologies become increasingly stringent, similar circuit design method as presented in this work should find wide range of applications for TL-based microwave circuits.

Acknowledgements

This work was partly supported by JSPS KAKENHI Grant Number 21K04181.

References

[1] F.H. Raab, "Class-F power amplifiers with maximally flat waveforms," IEEE Trans. Microw. Theory Techn., vol.45, no.11, pp.2007–2012, 1997.
[2] C.J. Wei, P. DiCarlo, Y.A. Tkachenko, R. McMorrow, and D. Bartle, "Analysis and experimental waveform study on inverse class-F mode of microwave power FETs," Proc. IEEE MTT-S Int. Microw. Symp., Boston, pp.525–528, 2000.
[3] N.O. Sokal and A.D. Sokal, "Class E-A new class of high-efficiency tuned single-ended switching power amplifiers," IEEE J. Solid-State Circuits, vol.10, no.3, pp.168–176, 1975.
[4] R. Ishikawa, Y. Takayama, K. Honjo, "Doherty amplifier design based on asymmetric configuration scheme," IEICE Trans. on Electron., vol.E104-C, no.10, pp.496–505, Oct. 2021.
[5] P. Colantonio, F. Giannini, R. Giofre, L. Piazzon, "Theory and experimental results of a class F AB-C Doherty power amplifier," IEEE Trans. Microw. Theory Techn., vol.57, no.8, pp.1936–1947, 2009.
[6] Z.A. Mokhti, P.J. Tasker, J. Lees, "Using waveform engineering to optimize class-F power amplifier performance in an envelope tracking architecture," Proc. European Micowave Integrated Circuits Conf., pp.1301–1304, Oct. 2014.
[7] K. Honjo, "A simple circuit synthesis method for microwave class-F ultra-high-efficiency amplifiers with reactance-compensation circuits," Solid-State Electron., vol.44, no.8, pp.1477–1482, 2000.
[8] A. Grebennikov, "High-efficiency class E/F lumped and transmission-line power amplifiers," IEEE Trans. Microw. Theory Techn., vol.59, no.6, pp.1579–1588, June 2011.
[9] K. Honjo, Y. Takayama, and R. Ishikawa, "General design theory for microwave power amplifiers and its applications," IEICE Trans. Electron. (Japanese version), vol.J97-C, no.12, pp.446–455, Dec. 2014.
[10] S. Tanaka, K. Saito, T. Oka, and Y. Shibosawa, "Applications of dispersion-engineered composite right-/left-handed transmission line stubs for microwave active circuits," IEICE Trans. Electron., vol.E100-C, no.10, pp.866–874, Oct. 2017.
[11] S. Tanaka, T. Oda, and K. Saiki, "2-GHz class-E power amplifier using a compact redundancy-free harmonic tuning circuit," Int. Journal of Microw. and Wireless Tech., vol.11, no.7, pp.618–624, July 2019.
[12] V. Carrubba et al., "The continuous class-F mode power amplifier," Proc. European Micowave Integrated Circuits Conf., pp.432–435, Oct. 2010.
[13] K. Chen and D. Peroulis, "Design of broadband highly efficient harmonic-tuned power amplifier using in-band continuous class-F^{-1}/F mode transferring," IEEE Trans. Microw. Theory Techn., vol.60, no.12, pp.4107–4116, Dec. 2012.
[14] S. Tanaka and H. Asami, "2-GHz class-E power amplifier using a compact redundancy-free harmonic tuning circuit," Proc. European Microwave Conference (EuMC2020), pp.13–16, Jan. 2021.
[15] M. Maeda, H. Masato, H. Takehara, M. Nakamura, S. Morimoto, H. Fujimoto, Y. Ota, and O. Ishikawa, ' "Source second-harmonic control for high efficiency power amplifiers," IEEE Trans. Microw. Theory Techn., vol.43, no.12, pp.2952–2957, Dec. 1995.
[16] J. Enomoto, R. Ishikawa, and K. Honjo, ' "Second harmonic treatment technique for bandwidth enhancement of GaN HEMT amplifier with harmonic reactive terminations," IEEE Trans. Microw. Theory Techn., vol.65, no.12, pp.4947–4952, 2017.
[17] P.J. Tasker and J. Benedikt, "Waveform inspired models and the harmonic balance emulator," IEEE Microw. Mag., vol.12, no.2, pp.38–54, April 2011.
[18] C. Caloz and T. Itoh, Electromagnetic Metamaterials: Transmission Line Theory and Microwave Applications, Wiley-IEEE Press, 2005.
[19] S. Tanaka, K. Mukaida, and K. Takata, "Compact stub resonators with enhanced Q-factor using negative order resonance modes of non-uniform CRLH transmission lines," IEICE Trans. Electron., vol.E98-C, no.3, pp.252–259, March 2015.

Shinichi Tanaka received the B.E. and M.E. degrees in Applied Physics from the University of Tokyo and the D.E degree in Electrical Engineering from Tohoku University in 1984, 1986 and 1997, respectively. In 1986, he joined the Central Research Laboratories, NEC Corporation, where he was involved in the development of GaAs and InP HBTs and their applications to microwave and millimeter-wave MMICs and high speed optical communication ICs. From 1992 to 1993, he was at Purdue University, West Lafayette, IN, as a Visiting Scholar. From 2005 to 2009, he was a Visiting Professor at the University of Electro-Communications, Tokyo. Since 2009, he has been a Professor at the Department of Information and Communications Engineering, Shibaura Institute of Technology, Tokyo. He was a co-recipient of the APMC'99 Microwave Prize. Dr. Tanaka is senior member of the IEEE and IEEJ.

Hirotaka Asami received the B.E. degree in Communications Engineering and the M.E. degree in Electrical Engineering and Computer Science from Shibaura Institute of Technology in 2018 and 2020, respectively. In 2020, he joined Transmission Devices Laboratory, Sumitomo Electric Industries, Ltd., where he is now involved in the development of next generation power amplifiers. Mr. Asami received the IEICE Electronics Society Student Award in 2019.

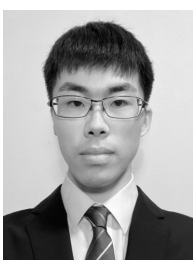

Takahiro Suzuki received the B.E. degree in information and Communications Engineering from Shibaura Institute of Technology in 2022. In 2022, he joined Mitsubishi UFJ Trust Systems Co., Ltd., Tokyo.